Investigation of DNA interaction and antiproliferative activity of mixed ligand dioxidomolybdenum(VI) complexes incorporating ONO donor aroylhydrazone ligands

Rupam Dinda*[,a], Arpita Panda,[a] Atanu Banerjee,[a] Monalisa Mohanty,[a] Sagarika Pasayat,[a] Edward. R. T. Tiekink[b]

[a]Department of Chemistry, National Institute of Technology, Rourkela, 769008 Odisha, India.

[b]Research Centre for Crystalline Materials, School of Science and Technology, 5 Jalan Universiti, Sunway University, Bandar Sunway, Selangor Darul Ehsan 47500, Malaysia

*Corresponding Author

E-mail: rupamdinda@nitrkl.ac.in (R. Dinda)

Tel.: + (91) 661 246 2657; Fax: + (91) 661 246 2022

ORCID ID: 0000-0001-9452-7791

Abstract

Four new mixed ligand dioxidomolybdenum(VI) [$Mo^{VI}O_2L^{1-3}(Q)$] **(1–3)**, [$Mo^{VI}O_2L^{4}(Q)]_2$ (H_2O) **(4)** [where Q = MeOH for **1** and imidazole for **2–4**] complexes have been synthesized using four different ONO donor aroylhydrazone ligands ($H_2L^{1–4}$). All the derived ligands and complexes were characterised by IR, UV-Vis, NMR spectroscopy and CHNS-analysis while the redox properties of the complexes have been investigated by cyclic voltammetry. The molecular geometries of **1–4** were established by X–ray crystallography and are closely related to each other, having a cis-$Mo(=O)_2$ core, a di-negative tridentate Schiff base ligand, which coordinates via the phenoxide-O1, amide-O4 and imine-N1 atoms, and with the sixth site occupied by an O-bound methanol molecule (**1**) or an N-bound imidazole molecule (**2–4**); **4** was isolated as a hydrate. The resultant NO_5 (**1**) and cis-N_2O_4 (**2–4**) donor sets are each based on a distorted octahedron. The complexes have been explored for their interaction with CT-DNA, where moderate binding constants were observed in the range 10^3 to 10^4 M^{-1}. The complexes showed different binding modes towards DNA such as intercalation, minor and major groove binding. Further, *in vitro* cytotoxicity activity of all the complexes were determined against HT-29 (colon cancer) and HeLa (cervical cancer) cell lines. Complex **4**, due to the presence of a heterocyclic 2-hydroxy-1-naphthyl moiety in the ligand backbone, was found to be comparatively more potent than the other complexes.

Keywords: Aroylhydrazone / Mixed ligand dioxidomolybdenum(VI) complexes / DNA binding/ Antiproliferative activity.

Introduction

Molybdenum is one of the major trace elements found in daily diet and is also found in three different enzymes present in humans namely, sulfite oxidase, xanthine oxidase and aldehyde oxidase that have functions in detoxification [1-4]. It has been reported that the lack of the required amount of molybdenum can increase the risk of esophageal cancer [5]. Studies showed cell-growth inhibition properties of various polyoxidomolybdates on some specific carcinoma cells, among which Mo(II) complexes produce good cytotoxicity results. Though there are few reports on molybdenum complexes as anticancer agents [6,7], it has been found that with increased chelation in the structure there is a decrease in anticancer properties [8]. Molybdenum can also be considered a better replacement for cisplatin compared to other transition metals, due its labile nature and comparatively low cytotoxicity against non-cancerous cells [9].

Molybdenum complexes of Schiff base ligands have gained significant interest owing to their low-cost and ease of preparation. Further, ligand preparation is basically facile: reacting sterically and electronically varied amines and aldehydes, respectively, through aldol condensation [10-20]. Schiff base ligands also have the potential to stabilize various metal ions in different oxidation states [21-25]. Moreover, the presence of a rigid, aromatic backbone provides specific spectroscopic properties that make transition metal complexes potential probes for nucleic acids. These metal complexes form intermediates in many enzymatic reactions that include the reaction of enzymes with amino or carbonyl group of the complex [26-40].

Aryl hydrazones form a class of Schiff base organic scaffolds which show a wide range of biological properties including anticonvulsant and antituberculosis properties along with others like antibacterial, antifungal, antiinflammatory, antinociceptive and antiplatelet activities [41-43]. Recently, Iproniazide, a hydrazone derived drug, has been used in the treatment of

tuberculosis [44]. Also, an oral nitrofuran antibiotic named Nifuroxazide is used for the treatment of anti-dehydration and for the treatment of colitis [45]. Furazolidone is a synthetic nitrofuran derivative that is well known for its antileishmanial activity and also clinically used as an antiprotozoal and antibacterial agent [46-50]. The advantageous electronic properties of arylhydrazones also give rise to complexes with more effective DNA-binding and DNA cleavage activities [27,32,34,35,37]. Molybdenum complexes of Schiff bases of aryl hydrazones are attractive due to their various applications including catalysis [51], luminescent probes [52], molecular sensors [53] and also display impressive biological activities [54-58] owing to the presence of the metal centre. On the other hand, as substituted imidazoles are found to have antiprotozoal, antifungal and antihypertensive properties [59-61], it has been employed as a co-ligand in the present study, in order to increase the overall biological potential of the synthesized complexes.

In the past few years, our research group has investigated the synthesis of several transition metal complexes incorporating –ONO and –ONS donor ligand systems in order to explore their biological activity [24, 62-77]. In continuation of this work, herein we report four novel dioxidomolybdenum(VI) complexes with –ONO donor, aroylazine ligand systems ($H_2L^{1–4}$). All the complexes are characterized by various spectroscopic methods and their structural features have been elucidated by X-ray crystallography. Furthermore, the complexes have been evaluated for their DNA interaction activity which shows a moderate binding affinity. Finally, the *in vitro* antiproliferative activities of **1–4** were assayed against the HT-29 (colon cancer) and HeLa (cervical cancer) cell lines and the mechanism of cell death for **4** ascertained by DAPI staining, i.e. apoptosis.

Experimental Section

Materials and Methods

The chemicals used herein were purchased from commercial sources, while the solvents were distilled under a dry nitrogen atmosphere according to the standard literature procedures [78, 79] prior to use. $[MoO_2(acac)_2]$ was used as the metal precursor and synthesized as per the reported procedure [79]. Elemental analysis (CHNS) measurements were carried out in a Vario EL cube elemental analyser instrument. FT–IR spectra were recorded by employing a Perkin Elmer Spectrum RX I spectrophotometer. Electronic spectra were recorded on a PerkinElmer Lambda 25 spectrophotometer. ^{1}H and ^{13}C NMR spectra where measured on a 400 MHz Bruker Ultrashield spectrometer with $SiMe_4$ as the standard. CH-Instruments (model no. CHI6003E) electrochemical analyser was used to analyse the redox behaviour with Pt as the working and auxiliary electrodes, saturated calomel electrode (SCE) as the reference electrode and TBAP (tetrabutylammonium perchlorate) (0.1M) as the supporting electrolyte under a dry nitrogen atmosphere at 298 K. Calf thymus (CT) DNA (biochemistry grade) was procured from SRL (India), methyl green, ethidium bromide, Dulbecco's phosphate buffered saline (DPBS), Dulbecco's modified Eagle medium (DMEM), fetal bovine serum (FBS), trypsin EDTA solution and antibiotic–antimitotic solution were procured from the Himedia (India). 3-[4,5-Dimethylthiazol-2-yl]- 2,5-diphenyltetrazolium (MTT) and 4′,6-diamidino-2-phenylindole dihydrochloride (DAPI) were purchased from Sigma-Aldrich (India). For the DNA binding study, ultrapure water used for the biological assay was obtained through the purification system Millipore MilliQ Academic.

Synthesis of ligands ($H_2L^{1–4}$)

Substituted aryl hydrazone ligands $H_2L^{1–3}$ were prepared by the condensation of 3-ethoxy-2-hydroxybenzaldehyde with the corresponding hydrazides [1-naphthoic hydrazide (H_2L^1), 2-furoic hydrazide (H_2L^2) and 2-thiophenecarboxylic acid hydrazide (H_2L^3)], while, H_2L^4 was

obtained by the condensation of 2-hydroxy-1-naphthaldehyde with isonicotinic hydrazide in equimolar ratio in EtOH medium by following standard procedures [24,65,74]. The resulting compounds were then filtered, washed thoroughly with ethanol and dried over fused $CaCl_2$ in a desiccator. Elemental analysis results NMR (^1H and ^{13}C), UV-Vis and IR data verified their preparation.

H_2L^1: Yield: 62%. Anal. calcd. for $C_{14}H_{14}N_2O_4$: C, 61.31; H, 5.14; N, 10.21. Found: C, 61.40; H, 5.36; N, 10.01. IR (KBr pellet, cm^{-1}): 3336 ν(O–H); 2998 ν(N–H); 1657 ν(C=O); 1556 ν(C=N). ^1H NMR (400 MHz, DMSO-d_6): δ 12.13 (s, 1H,–OH), 10.81 (s, 1H, NH), 8.65 (s, 1H, HC=N–), 7.97–6.72 (m, 6H, aromatic), 4.06 (m, 2H, $–OCH_2$), 1.35 (t, 3H, $–CH_3$). ^{13}C NMR (100 MHz, DMSO-d_6): δ 166.18 (CO–N), 159.18 (N=CH–), 152.36–113.59 (10C, aromatic), 69.33 ($–OCH_2$), 19.95 ($–CH_3$).

H_2L^2: Yield: 71%. Anal. calcd. for $C_{20}H_{18}N_2O_3$: C, 71.84; H, 5.43; N, 8.38. Found: C, 71.78; H, 5.42; N, 8.41. IR (KBr pellet, cm^{-1}): 3392 ν(O–H); 3042 ν(N–H); 1657 ν(C=O); 1571 ν(C=N). ^1H NMR (400 MHz, DMSO-d_6): δ 12.02 (s, 1H,–OH), 10.62 (s, 1H, NH), 9.13 (s, 1H, HC=N–), 8.02–6.97 (m, 10H, aromatic), 4.07 (m, 2H, $–OCH_2$), 1.35 (t, 3H, $–CH_3$). ^{13}C NMR (100 MHz, DMSO-d_6): δ 169.16 (CO–N), 158.67 (N=CH–), 154.16–118.21 (16C, aromatic), 68.31 ($–OCH_2$), 14.56 ($–CH_3$).

H_2L^3: Yield: 74%. Anal. calcd. for $C_{14}H_{14}N_2O_3S$: C, 57.92; H, 4.86; N, 9.65; S, 11.04. Found: C, 57.83; H, 4.91; N, 9.64; S, 10.99. IR (KBr pellet, cm^{-1}): 3378 ν(O–H); 2998 ν(N–H); 1663 ν(C=O); 1561 ν(C=N). ^1H NMR (400 MHz, DMSO-d_6): δ 12.11 (s, 1H,–OH), 10.86 (s, 1H, NH), 8.86 (s, 1H, HC=N–), 7.92–6.98 (m, 6H, aromatic), 4.06 (m, 2H, $–OCH_2$), 1.35 (t, 3H, $–CH_3$). ^{13}C NMR (100 MHz, DMSO-d_6): δ 167.02 (CO–N), 156.23 (N=CH–), 151.52–115.23 (10C, aromatic), 66.34 ($–OCH_2$), 16.52 ($–CH_3$).

H_2L^4: Yield: 74%. Anal. calcd. for $C_{17}H_{15}N_3O_2$: C, 69.61; H, 5.15; N, 14.33. Found: C, 69.24; H, 5.44; N, 14.41. IR (KBr pellet, cm^{-1}): 3389 ν(O–H); 2988 ν(N–H); 1653 ν(C=O); 1569

ν(C=N). ^{1}H NMR (400 MHz, DMSO-d_6): δ 12.53 (s, 1H,–OH), 12.41 (s, 1H, NH), 9.49 (s, 1H, HC=N–), 8.85–7.24 (m, 10H, aromatic). ^{13}C NMR (100 MHz, DMSO-d_6): δ 166.89 (CO–N), 160.41 (N=CH–), 151.52–114.91(13C, aromatic).

Synthesis of (1)

$[MoO_2(acac)_2]$ was added to an refluxing solution of H_2L^1 (1:1 ratio) taking methanol as the solvent. The reaction mixture was refluxed for 4 h after which the solution turned dark-orange. The resultant reaction mixture was filtered and kept for crystallization. After 2-3 days of slow evaporation, a fine orange crystalline complex, $[Mo^{VI}O_2L^1(Q)]$ (where, Q = MeOH) (**1**), suitable for X-ray crystallographic measurements was obtained.

$[Mo^{VI}O_2L^1(Q)]$ (1): Yield: 66%. Anal. Calcd for $C_{15}H_{16}MoN_2O_7$: C, 41.68; H, 3.73; N, 6.48; Found: C, 41.66; H, 3.79; N, 6.51. IR (KBr pellet, cm−1): 1584 ν(C=N), 945, 934 ν(Mo=O). UV−Vis (DMSO): λmax, nm (ε, $dm^3\ mol^{-1}\ cm^{-1}$): 442 (1011), 310 (9758). ^{1}H NMR (400 MHz, DMSO-d_6): δ (ppm): 8.89 (s, 1H, HC=N–), 7.96–6.71 (m, 6H, aromatic), 4.14 (s, 1H, –HO (enolic)), 4.096 (m, 2H, –OCH_2), 3.18 (d, 3H, –OCH_3), 1.35 (t, 3H, –CH_3). ^{13}C NMR (100 MHz, DMSO-d_6): δ (ppm): 161.98 (CO=N), 156.32 (N=CH–), 149.78–112.98 (10C, aromatic), 64.82 (–OCH_2), 49.07 (–OCH_3), 15.19 (–CH_3).

Synthesis of mixed-ligand complexes (2–4)

The precursor $[MoO_2(acac)_2]$ was added to an refluxing methanolic solution of $H_2L^{2\text{-}4}$ in a equimolar ratio and a dark-orange solution was obtained in each case after 1 h of reflux. Then a stoichiometric amount of the co-ligand imidazole (Q) was added. Each solution was filtered after a reflux period of ca 3 h. After slow evaporation of the filtrate over 4 days, orange-red crystals of $[Mo^{VI}O_2L^{2\text{-}3}(Q)]$ (**2** and **3**) and $[Mo^{VI}O_2L^4(Q)]_2(H_2O)$ (**4**), were obtained and washed thoroughly with methanol and dried.

$[Mo^{VI}O_2L^2(Q)]$ (2): Yield: 68%. Anal. Calcd for $C_{23}H_{22}MoN_4O_5$: C, 52.28; H, 3.82; N, 10.60. Found: C, 52.17; H, 3.88; N, 10.71. IR (KBr pellet, cm−1): 1567 ν(C=N); 922, 906 ν(Mo=O).

UV−Vis (DMSO): λmax, nm (ε, $dm^3\ mol^{-1}\ cm^{-1}$): 441 (1300), 307 (10124). ^{1}H NMR (400 MHz, DMSO-*d*$_6$): δ (ppm): 9.06 (s, 1H, HC=N–), 8.83–7.02 (m, 13H, aromatic), 4.12 (m, 2H, –OCH_2), 1.38 (t, 3H, –CH_3). ^{13}C NMR (100 MHz, DMSO-d_6): *δ* (ppm): 170.78 (CO=N), 157.32 (N=CH–), 150.10–119.24 (19C, aromatic), 64.83 (–OCH_2), 15.22 (–CH_3).

[$Mo^{VI}O_2L^3$(Q)] (3): Yield: 64%. Anal. Calcd for $C_{17}H_{16}MoN_4O_5S$: C, 42.16; H, 3.33; N, 11.57; S, 6.62. Found: C, 42.11; H, 3.39; N, 11.58; S, 6.71. IR (KBr pellet, cm−1): 1557 ν(C=N); 928, 906 ν(Mo=O). UV−Vis (DMSO): λmax, nm (ε, $dm^3\ mol^{-1}\ cm^{-1}$): 442 (1425), 322 (8986). ^{1}H NMR (400 MHz, DMSO-*d*$_6$): δ (ppm): 8.87 (s, 1H, HC=N–), 7.86–6.99 (m, 6 H, aromatic), 4.07 (m, 2H, –OCH_2), 1.34 (t, 3H, –CH_3). ^{13}C NMR (100 MHz, DMSO-d_6): *δ* (ppm): 165.90 (CO=N), 155.69 (N=CH–), 150.27–119.71 (10C, aromatic), 65.22 (–OCH_2), 15.19 (–CH_3).

[$Mo^{VI}O_2L^4$(Q)]$_2$ (H_2O) (4): Yield: 61%. Anal. Calcd for $C_{40}H_{32}Mo_2N_{10}O_9$: C, 48.60; H, 3.26; N, 14.17. Found: C, 48.66; H, 3.21; N, 14.18. IR (KBr pellet, cm−1): 1557 ν(C=N); 928, 906. ν(Mo=O). UV−Vis (DMSO): λmax, nm (ε, $dm^3\ mol^{-1}\ cm^{-1}$): 453 (2983), 328 (9456), 260 (10531). ^{1}H NMR (400 MHz, DMSO-*d*$_6$): δ (ppm): 9.82 (s, 1H, HC=N–), 8.79–7.03 (m, 13 H, aromatic). ^{13}C NMR (100 MHz, DMSO-d_6): *δ* (ppm): 166.87 (CO=N), 161.33 (N=CH–), 154.31–112.00 (16C, aromatic).

Single crystal X-ray structure determination

Crystal data and refinement details for **1**-**4** are collated in Table 1. Intensity data (100 K) for **1**-**3** were measured on a Rigaku/Oxford Diffraction XtaLAB Synergy diffractometer (Dualflex, AtlasS2) fitted with CuKα radiation (λ = 1.54178 Å) while those for **4** were measured on an Agilent Technologies SuperNova Dual CCD with an Atlas detector fitted with Mo Kα radiation (λ = 0.71073 Å). Data reduction and empirical absorption corrections, based on a gaussian (**1**-**3** [80]) or multi-scan (**4** [81]) techniques, were applied. The structures were solved by direct methods [82] and refined on F^2 with anisotropic displacement parameters and C-bound H

atoms in the riding model approximation [83]. For **1**, the oxygen-bound H atoms were refined with a distance restraint O–H = 0.84±0.01 Å while for **2**-**4**, the nitrogen-bound H atoms were refined with a distance restraint N–H = 0.88±0.01 Å. A weighting scheme of the form $w = 1/[\sigma^2(F_o^2) + (aP)^2 + bP]$ where $P = (F_o^2 + 2F_c^2)/3)$ was introduced in each refinement. For **2**, the maximum and minimum residual electron density peaks of 2.69 and 1.03 eÅ^{-3}, respectively, were located 0.84 and 0.72 Å from the Mo atom, respectively. This is an artefact of the data and not indicative of unresolved chemistry. For **3**, owing to poor agreement, the (1 1 3) reflection was omitted from the last cycles of refinement. The thienyl ring was disordered over two co-planar, anti-parallel orientations with the site occupancy factor of the major component refining to 0.875(4). The C9, C11 and C12 positions were common to both components and were refined anisotropically. The S1 and C10 atoms of the major component were refined anisotropically but those for the minor component were refined isotropically. The C9–C10 and C10–C11 bond lengths of the minor component were constrained to be equivalent to those for the major component. Finally, the absolute structure was determined based on differences in Friedel pairs included in the data set. In **4**, there is half a water molecule disordered over two positions about a centre of inversion; the O–H distances were fixed at 0.84 Å. There is some evidence for disorder in the imidazole ring as seen in the shapes of the displacement ellipsoids. However, an alternate position was not discerned for this molecule. The molecular structure diagrams were generated by ORTEP for Windows [84] and the packing diagrams with DIAMOND [85]. Additional data analysis was made with PLATON [86].

Table 1. Crystal data and refinement details for complexes **1**-**4**.

Complex	**1**	**2**	**3**	**4**
Formula	$C_{15}H_{16}MoN_2O_7$	$C_{23}H_{20}MoN_4O_5$	$C_{17}H_{16}MoN_4O_5S$	$C_{40}H_{32}Mo_2N_{10}O_9$
Formula weight	432.24	528.37	484.34	988.64
Crystal colour	light-brown	light-brown	light-brown	red-brown
Crystal size/mm^3	0.08 × 0.10 × 0.11	0.03 × 0.04 × 0.08	0.13 × 0.16 × 0.17	0.10 × 0.25 × 0.30
Crystal system	Triclinic	Triclinic	Orthorhombic	Monoclinic
Space group	$P\bar{1}$	$P\bar{1}$	$P2_12_12_1$	$P2_1/n$
a/Å	10.2487(2)	7.98370(10)	8.09320(10)	9.4568(2)
b/Å	12.2450(2)	9.8896(2)	12.0195(2)	13.0259(2)
c/Å	13.2350(4)	13.9897(2)	19.6535(2)	15.9707(3)
α/°	90.236(2)	91.2290(10)	90	90
β/°	97.070(2)	90.0870(10)	90	106.320(2)
γ/°	90.6870(10)	104.721(2)	90	90
V/Å^3	1648.16(7)	1068.03(3)	1911.82(4)	1888.05(6)
Z	4	2	4	2

1	D_c/g cm^{-3}	1.742	1.643	1.683	1.739
2	F(000)	872	536	976	996
3	μ(MoKα)/mm^{-1}	6.901	5.410	6.972	0.738
4	Measured data	39123	25342	13028	9628
5	θ range/°	3.4 – 67.1	3.2 – 67.1	4.3 – 67.1	2.3 – 29.3
6	Unique data	5893	3817	3399	4403
7	Observed data ($I \geq 2.0\sigma(I)$)	5652	3707	3386	3665
8	No. parameters	461	302	266	283
9	R, obs. data; all data	0.022; 0.059	0.037; 0.096	0.019; 0.047	0.031; 0.074
10	a; b in weighting scheme	0.039; 1.022	0.052; 2.843	0.030; 0.698	0.037; 2.383
11	R_w, obs. data; all data	0.023; 0.600	0.038; 0.097	0.019; 0.047	0.043; 0.083
12	Range of residual electron				
13	density peaks/eÅ^{-3}	-0.74 – 0.42	-1.03 – 2.69	-0.65 – 0.26	-0.57–0.63

DNA binding experiments

Absorption spectral studies

Interaction of the dioxidomolybdenum(VI) complexes with CT-DNA was studied through UV-Vis absorption titration experiments. A fixed concentration of the metal complex (25 μM) was titrated against a variable concentration of CT-DNA (0 to 110 μM) in 50 mM Tris-HCl buffer (pH 8.0). Readings were recorded after each addition of CT-DNA (10 μM) to the metal. Data were then calculated using the following equation (Eqn 1) to obtain the binding constant K_b [37,66,73]

$$\frac{[DNA]}{\varepsilon_a - \varepsilon_f} = \frac{[DNA]}{\varepsilon_b - \varepsilon_f} + \frac{1}{K_b(\varepsilon_b - \varepsilon_f)} \quad \text{(Eqn 1)}$$

where [DNA] is represents the concentration of CT–DNA base pairs whereas the parameters ε_a, ε_f and ε_b correspond to the apparent extinction co-efficient for the complexes, i.e. Abs/[complex] in the presence and absence of CT–DNA and to fully bound DNA, respectively. A plot of [DNA]/($\varepsilon_a - \varepsilon_f$) vs [DNA] gave a slope of 1/($\varepsilon_a - \varepsilon_f$) and the intercept equal to (1/K_b)($\varepsilon_b - \varepsilon_f$). Thus, the ratio of the slope to the intercept gives the value of binding constant K_b. Binding affinity of the ligands towards CT-DNA was studied in a similar fashion by taking a fixed concentration of ligand [25 μM in 50 mM Tris-HCl buffer (pH 8.0)] against variable CT-DNA concentrations ranging from 0 to 100 μM.

Competitive DNA binding by Fluorescence measurements

To understand the exact mode of binding of the complexes with CT-DNA, competitive DNA binding experiments with three fluorescent dyes namely 4′,6-diamidino-2-phenylindole (DAPI), methyl green (MG) and ethidium bromide (EB) was carried out. Among these fluorescent dyes EB tends to bind DNA through intercalation whereas DAPI and MG bind to the minor and major grooves, respectively [66,87,88]. This was studied by measuring the fluorescence emission intensities of DAPI, MG and EB bound CT-DNA at 455 nm (excitation 358 nm), 663 nm (excitation 600 nm) and 597 nm (excitation 520 nm) with an increasing

amount of the complex concentration (0−100 μM) in a Fluoromax 4P spectrofuorimeter (Horiba Jobin Mayer, USA).

***In vitro* cytotoxic activity**

Cell cultures

HT-29 (colon cancer) and HeLa (cervical cancer) cells were obtained from National Centre of Cell Science (NCCS), Pune, India. The cells were maintained in DMEM supplemented with 10% FBS and penicillin–streptomycin solution at 37 °C in a 95% humidified and 5% CO_2 incubator. Working concentrations of 5, 10, 50 and 100 μg/ml were prepared in culture medium from a stock concentration of 3 mg/ml of each complex. Also, the concentration of DMSO was maintained at less than 0.1% (v/v) in all experiments to avoid any toxicity due to DMSO.

MTT assay

For the MTT assay, both HT-29 and HeLa cells were harvested from their maintenance cultures in logarithmic phase. Following cell counting in a hemocytometer, cells were seeded into a 96 well plate, at a concentration of 1×10^4 cells per well. These cells were then incubated with various concentrations of the test compounds for 48 h. The result of the treatment of the complexes on viability of the cancer cells was studied using MTT dye reduction assay by measuring the optical density at 595 nm using micro-plate reader spectrophotometer (Perkin-Elmer 2030) [78].

DAPI staining

Nuclear morphology of the cancer cells in response to treatment with the complexes was studied through DAPI staining by following a reported procedure [68]. Treated and untreated cells were fixed with 4 % formaldehyde for 15 min followed by staining with 1 μg/ml DAPI for 5 min at 37 °C. The cells were then washed with PBS and finally examined by fluorescence microscopy (Olympus IX 71) to determine if any nuclear condensation or fragmentation had occurred, indicating the cells underwent apoptosis.

Results and discussion

Synthesis

In the present study, four new mixed ligand dioxidomolybdenum(VI) $[Mo^{VI}O_2L^{1-3}(Q)]$ **(1–3)**, $[Mo^{VI}O_2L^{4}(Q)]_2$ (H_2O) **(4)** [where Q = MeOH for **1** and imidazole for **2–4**] complexes were synthesized from four differently substituted ONO donor aroylhydrazone ligands, $H_2L^{1–4}$, as indicated in Scheme 1. The complexes were successfully characterized by UV−vis, IR, NMR, cyclic voltammetry and the molecular and crystal structures were determined by X-ray crystallography. The aqueous phase stability of the complexes has been investigated by time-dependent UV-vis spectroscopy for 72h and a representative spectrum, for **1**, is depicted in Fig. SI 1.

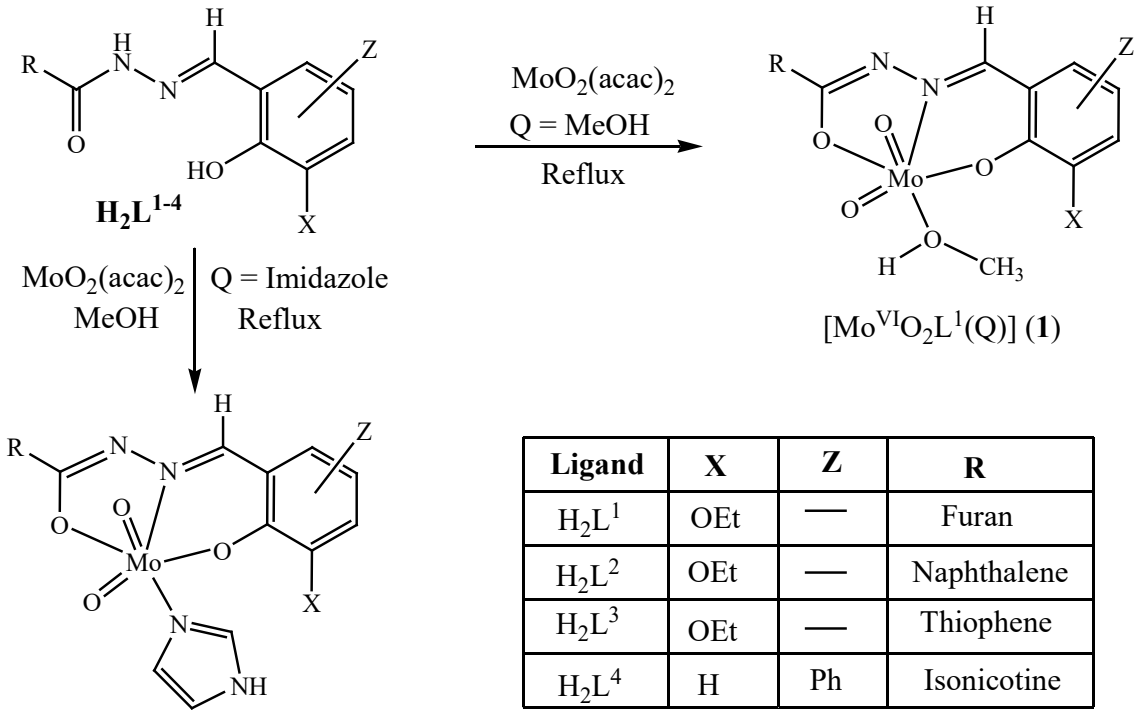

Ligand	X	Z	R
H_2L^1	OEt	—	Furan
H_2L^2	OEt	—	Naphthalene
H_2L^3	OEt	—	Thiophene
H_2L^4	H	Ph	Isonicotine

Scheme 1. Schematic pathway for the formation of $[Mo^{VI}O_2L^{1-3}(Q)]$ **(1–3)**, $[Mo^{VI}O_2L^{4}(Q)]_2$ (H_2O) **(4)**.

Spectral characteristics

Detailed spectral (IR, UV-Vis and NMR) data of H_2L^{1-4} and their respective corresponding complexes (**1**–**4**) are given in the *Experimental section*. Infrared spectra of the ligands display three broad band in the ranges 3392–3336, 3042–2988 and 1663–1653 cm^{-1} which are attributed to *ν*(O–H) stretching of hydroxy group of 2-hydroxy aldehyde, *ν*(N–H) stretching and *ν*(C=O) stretching, respectively. Disappearance of characteristic bands of O–H, N–H and C=O in the complex spectra indicates the coordination of the ligands to the metal centre in their phenolate form after enolization [77,89]. Also, the presence of two new stretching bands in the range 928–906 cm^{-1} in the complex spectra indicate the dioxido nature (Mo=O) of the complexes.

Electronic spectra of **1**–**4** were recorded in DMSO. The spectra of all the complexes were similar in nature and as a representative UV-Vis spectrum of **4** is depicted in Fig. 1. Strong absorptions observed in the range 453–442 nm are assignable to ligand-to-metal charge transfer (LMCT) transitions whereas bands in the higher energy region 328–260 nm are likely to be due to ligand centred transitions [75,77]. Moreover, the presence an extra peak in the complex spectra at 453–442 nm region, as compared to that of the ligand suggests coordination of the ligand upon complexation.

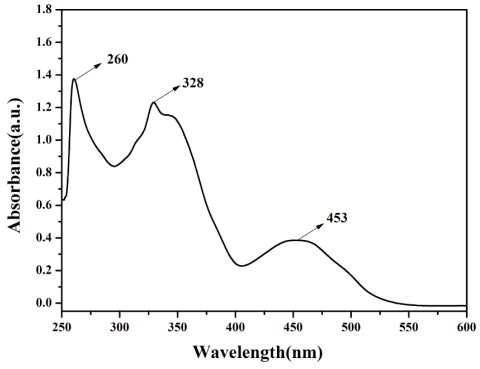

Fig. 1. UV-vis spectra of $[Mo^{VI}O_2L^4(Q)]_2.H_2O$ (**4**) in DMSO employing the complex concentration 1.3×10^{-4} M.

The ^{1}H and ^{13}C NMR data of $H_2L^{1–4}$ and their corresponding complexes (**1**–**4**) were recorded in DMSO-d_6. The ligand spectra exhibit two singlets in the ranges δ = 12.53–12.02 and 12.41–10.62 ppm due to the presence of phenolic –OH and NH protons, respectively. The disappearance of these two resonances in the spectra of the complexes confirms their deprotonation and coordination to the central metal atom. The presence of a singlet resonance for the ligands and complexes in the region δ = 9.82–8.65 ppm is attributed to the azomethine –CH proton. One quartet in the range δ = 4.12–4.06 ppm and a triplet in the range δ = 1.38–1.34 ppm is observed for $H_2L^{1–3}$ and their complexes **1**–**3** due to the presence of the ethoxy group in the ligand moiety. On the other hand, due to presence of a coordinated MeOH molecule, complex **1** exhibits an OH (enolic) resonance at δ = 4.14 ppm and a $–OCH_3$ resonance at δ = 4.09 ppm. Moreover, the increased number of resonances in the aromatic region for ~~complexes~~ **2**–**4** as compared to $H_2L^{2–4}$ indicates the binding of co-ligand imidazole to the metal atom. ^{1}H NMR spectra of all the complexes (**1**–**4**) are given in Figs SI 2–5.

In the ^{13}C NMR spectra of **1**–**4**, signals for the aromatic carbons are found in the downfield region in the range δ = 170.78–112.98 ppm. Signals for the aliphatic carbons of $–OCH_2$ and $–CH_3$ of **1**–**3** appear in the range δ = 65.22–15.19 ppm. Whereas complex **1** exhibits an additional aliphatic carbon signal at δ = 49.07 due to the presence of methanolic $–OCH_3$ carbon.

Electrochemical Properties

Electrochemical properties of the complexes have been studied by cyclic voltammetry in DMSO solution. Voltammograms of all the complexes show a similar type of redox property and representative voltammograms for **1** and **2** are depicted in Fig. 2. An irreversible single electron reductive response is observed in the cathodic region at a potential window −0.74 to −0.69 V that can be attributed to the Mo(VI) → Mo(V) reduction [68,74,76,90]. Also, a single electron irreversible cathodic response in the region −1.04 to −0.95 V and anodic response at a potential window 0.44 to 0.12 V are observed that may be attributed to the ligand centered

reduction and oxidation, respectively. The cyclic voltammetry experiments of the ligands have also been performed and a representative voltammogram of H_2L^1 is shown in Fig. SI 6. The redox potential data of all the complexes are listed in Table 2 and the single electron processes were also confirmed by comparing the current height to the standard ferrocene−ferrocenium couple under identical experimental conditions.

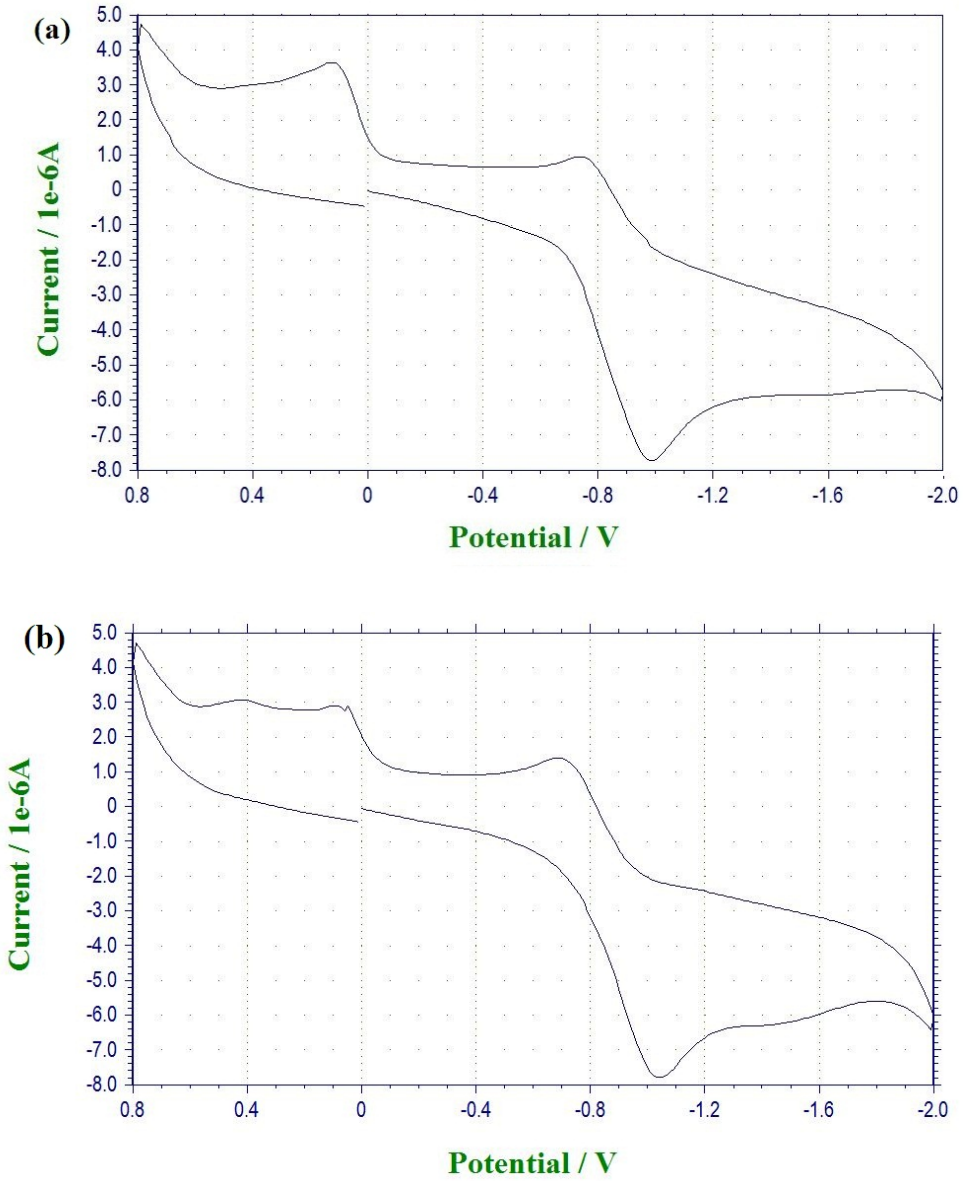

Fig. 2. Cyclic voltammogram of $[Mo^{VI}O_2L^1(Q)]$ (**1**) (**a**) and $[Mo^{VI}O_2L^2(Q)]$ (**2**) (**b**) in DMSO.

Table 2. Cyclic voltammetric results[a] for **1**–**4** at 298 K in DMSO.

Complex	E^{c}_{P} (V)	E^{a}_{P} (V)
1	−0.74, −0.99	0.12
2	−0.69, −1.04	0.39
3	−0.71, −1.04	0.21
4	−0.70, −0.95	0.44

[a] In DMSO at a scan rate 100 mV s^{-1}. Where E^{c}_{P} and E^{a}_{P} are cathodic and anodic peak potentials vs. SCE, respectively.

Molecular structures

The molecular structures of **1**-**4** have been established by X-crystallography and selected geometric parameters are collated in Table 3. The crystallographic asymmetric unit of **1** comprises two independent molecules, the first of which is shown in Fig. 3(a) and the second in Fig. SI 7(a); the molecules have very similar conformations as seen in the overlay diagram of Fig. SI 7(b). The molecules of **1** comprise a $Mo(=O)_2$ core complexed by a di-negative, tridentate Schiff base ligand, via the phenoxide-O1, amide-O4 and imine-N1 atoms, with the sixth site occupied by an O-bound methanol molecule. The oxo groups are cis, the phenoxide-O1 and amide-O4 atoms trans, the oxido-O2 atom, occupying a position in the approximate plane of the tridentate ligand, is trans to the imine-N1 atom, and the oxido-O3 atom is trans to the methanol-O6 atom. The resulting NO_5 donor set is based on an octahedron. The mode of coordination of the tridentate ligand gives rise to five- and six-membered chelate rings and it is the acute bite angles subtended by these (Table 3) that are responsible for the major distortions from the ideal octahedral geometry.

The Mo-O1(phenoxide) bond length of 1.9170(14) Å is considerably shorter than the Mo-O4(amide) bond length of 2.0299(14) Å, an observation correlated with delocalisation of π-electron density over the amide chromophore. ~~While the differences in the geometric~~

~~parameters involving the lighter atoms are small, there are discernible and consistent trends to substantiate this observation. Thus, the C8–O4 bond length is significantly shorter than the C1–O1 bond, i.e. 1.312(2) Å cf. 1.351(2) Å, and conversely, there is an indication the formally double C8–N2 bond is longer, at 1.309(3) Å, than the C7–N1 imine bond, at 1.295(3) Å, the experimental errors notwithstanding. In the same way, there is an indication that the Mo–O2(oxido) bond length is longer than the Mo–O3(oxido) bond, i.e. 1.7083(13) Å cf. 1.6956(15) Å, with the former being trans to the imine-N1 atom, and the latter trans to the methanol-O6 atom.~~ Delete to make the text shorter? I obviously think this is important but, perhaps it is too detailed for the Journal's liking

As mentioned above, the five-membered, i.e. Mo,O4,N1,N2,C8, and six-membered, i.e. Mo,O1,C1,C6,C7,N1, chelate rings are formed upon complexation of the di-anion. The five-membered ring is practically planar, exhibiting a r.m.s. deviation for the five atoms of 0.0087 Å. By contrast, the best description for the six-membered ring is that of an envelope whereupon the Mo1 atom lies 0.504(2) Å out of the plane of the five remaining atoms, which exhibit a r.m.s. deviation of 0.0435 Å. The dihedral angle between the least-squares planes through the chelate rings is 7.82(9)°, indicating the backbone of the tridentate ligand is approximately planar. The appended furanyl ring makes a dihedral angle of 6.11(13)° with the five-membered chelate ring, again indicating a co-planar arrangement; the dihedral angle between the outer rings is 5.26(14)°.

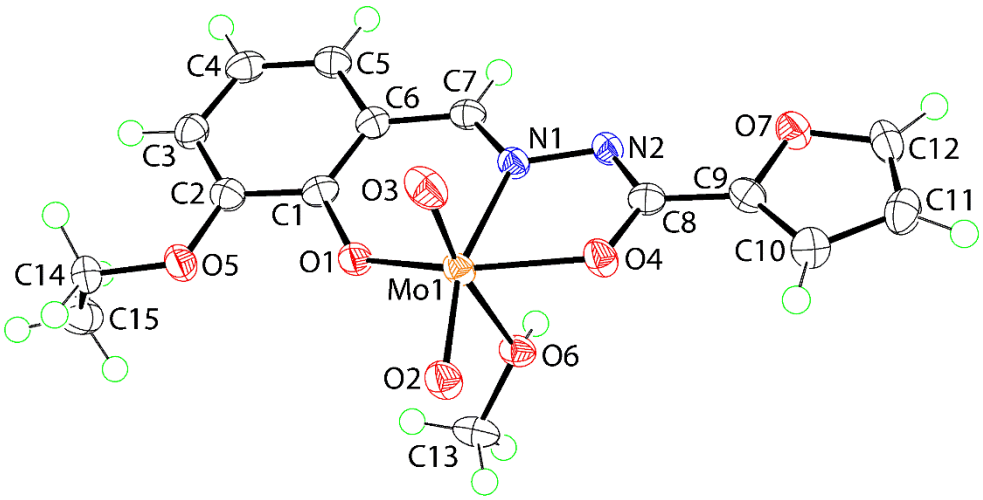

Fig. 3. Molecular structure of the first independent molecule comprising the asymmetric unit of **1**, showing the atom labelling scheme and anisotropic displacement parameters at the 70% probability level.

Table 3. Selected geometric parameters (Å, °) for complexes **1**-**4**.

Complex	**1**	**1** [a]	**2**	**3**	**4**
	(Y = O6)	(Y = O6)	(Y = N3)	(Y = N3)	(Y = N3)
Parameter					
Mo–O1	1.9170(14)	1.9242(14)	1.947(2)	1.947(2)	1.9367(17)
Mo–O2	1.7083(13)	1.7068(13)	1.714(3)	1.709(2)	1.7064(18)

Mo–O3	1.6956(15)	1.6966(15)	1.701(3)	1.698(2)	1.7040(19)
Mo–O4	2.0299(14)	2.0351(14)	2.010(2)	2.016(2)	2.0169(19)
Mo–N1	2.2457(16)	2.2423(16)	2.231(3)	2.248(2)	2.228(2)
Mo–Y	2.3207(14)	2.3221(14)	2.347(3)	2.330(2)	2.336(2)
O1–C1	1.351(2)	1.347(2)	1.357(4)	1.353(4)	1.343(3)
O4–C	1.312(2)	1.314(2)	1.327(4)	1.322(4)	1.320(3)
N1–N2	1.395(2)	1.391(2)	1.403(4)	1.393(3)	1.403(3)
N1–C	1.295(3)	1.296(3)	1.275(5)	1.296(4)	1.291(3)
N2–C	1.309(3)	1.308(3)	1.293(5)	1.307(4)	1.297(3)
O1–Mo–O4	150.17(6)	149.39(6)	149.59(10)	149.33(8)	148.77(8)
O1–Mo–N1	81.27(6)	80.85(6)	81.66(10)	81.61(9)	80.41(7)
O2–Mo–O3	106.63(7)	105.78(7)	105.94(13)	104.69(10)	106.42(10)
O2–Mo–N1	157.75(6)	157.86(6)	161.21(12)	163.61(9)	161.96(9)
O3–Mo–Y	169.24(6)	171.72(6)	169.43(12)	170.54(10)	168.97(9)
O4–Mo–N1	72.09(6)	71.49(5)	71.77(10)	71.93(9)	72.25(7)

[a] The parameters for the second independent molecule in **1** follow the numbering scheme shown in Fig. 3(a).

~~The second molecule comprising the asymmetric of **1** adopts essentially the same molecular structure and trends as for the first. The envelope conformation for the six-membered ring is more pronounced with the Mo2 atom lying 0.603(2) Å out of the plane of the five remaining atoms (r.m.s. deviation = 0.0367 Å). The dihedral angle between the chelate rings is 9.45(9)°, between the five-membered and furanyl rings 3.02(12)° and between the outer rings 13.67(12)°, mirroring the first independent molecule~~. and/or delete this?

The molecular structures of **2** and **3** are closely related to that of **1** in that the methanol molecule has been replaced by an imidazole in each case, and with the furanyl substituent in **1** replaced by naphthyl (**2**) and thienyl (**3**), leading to cis-N_2O_4 distorted octahedral geometries. In **4**, imidazole is still present but both peripheral aromatic systems differ, being based on naphthyl and 4-pyridyl; **4** was isolated as a mono-hydrate. The molecular structures of **2**-**4** are shown in

Figs 4(a)-(c) and selected geometric parameters are given in Table 3. The molecular geometry and trends in geometric parameters for **2**-**4** match closely those established for **1**. The notable exception is the equivalence of the Mo-O(oxido) bond lengths in **4**. The conformations of the chelate rings also match those seen in **1**; geometric data are given in Table SI 1. Across the series, the five-membered rings are most planar in the structures of **2** and **3**, and in terms of the deviations of the Mo atoms in the envelope conformations for the six-membered rings, these are intermediate to those seen in the independent molecules of **1**. In the same way, the dihedral angles between the chelate rings in each of **2**-**4** are intermediate to those seen in **1**. The dihedral angles between the outer aromatic rings is greater than those in **1** in the case of **2**, i.e. 14.77(11)°, or smaller, in **3** (2.13(17)°) and **4** (4.77(19)°).

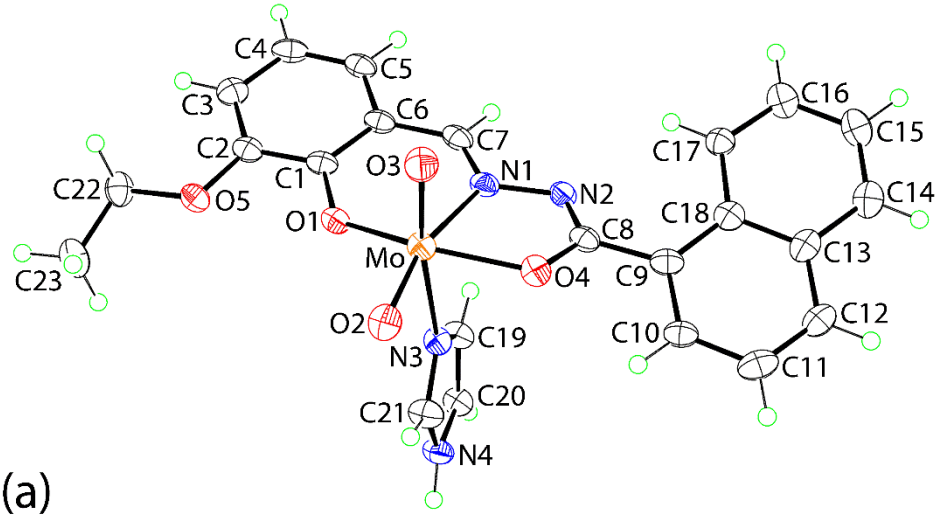
C4
C5
C3
C6
C7
C2
C1
O3
N1
N2
C22
O5
O1
C8
Mo
O4
C9
C23
O2
C19
C10
N3
C11
C21
C20
N4
C16
C15
C17
C14
C18
C13
C12

(a)

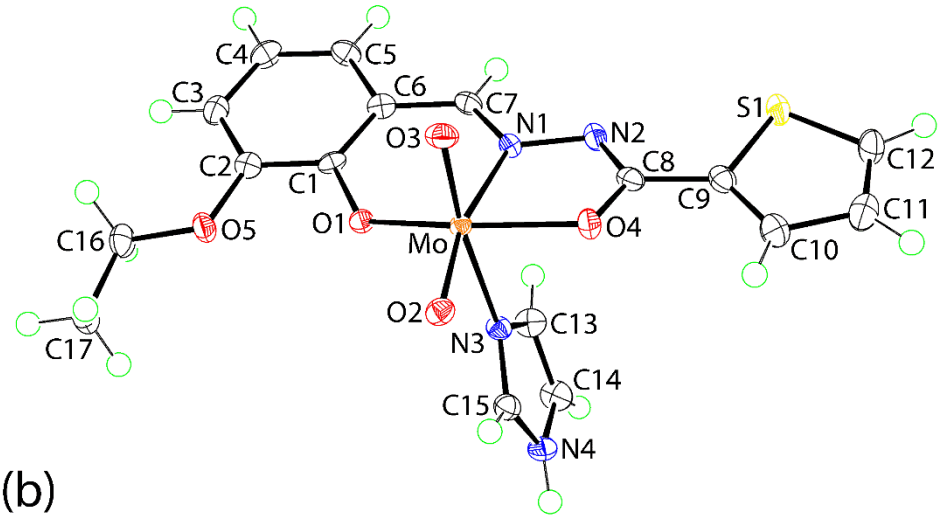
C4
C5
C3
C6
C7
N1
N2
S1
O3
C2
C1
C8
C9
C12
C11
O5
O1
Mo
O4
C10
C16
O2
C13
N3
C17
C14
C15
N4

(b)

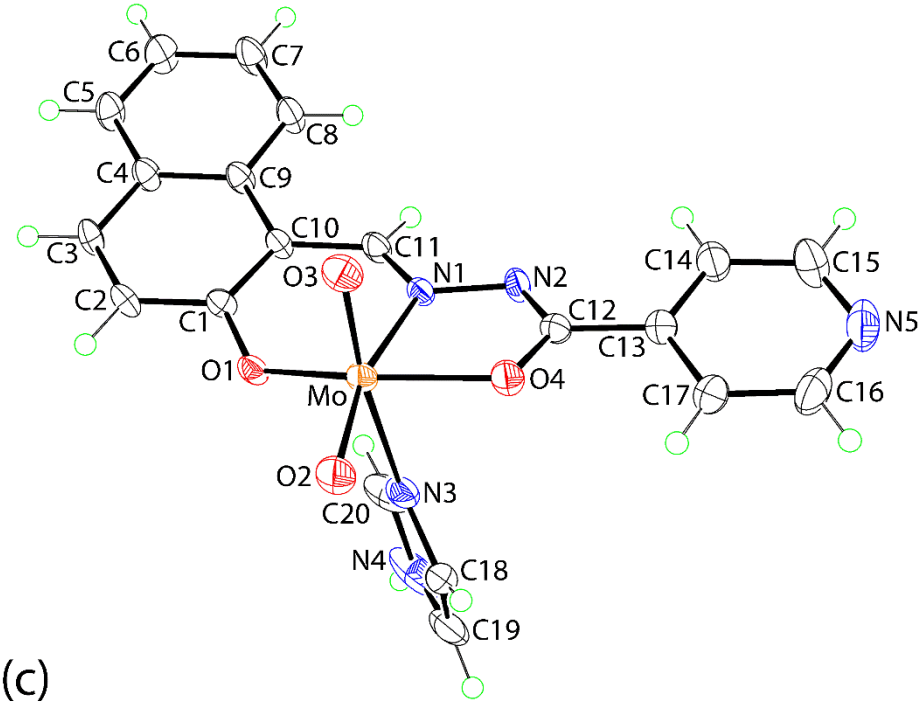
C6
C7
C5
C8
C4
C9
C10
C11
C3
O3
N1
N2
C14
C15
C2
C1
C12
N5
C13
O1
Mo
O4
C17
C16
O2
N3
C20
N4
C18
C19

(c)

1

Fig. 4. Molecular structures of (a) **2**, (b) **3** (minor component of the disordered thienyl ring is omitted) and (c) **4** (water molecule omitted) showing atom labelling schemes and displacement parameters at the 50, 70 and 50% probability levels, respectively.

Molecular packing

The geometric parameters associated with the specified intermolecular interactions discussed in the following are collated in the respective captions of Figs 5 and SI 8-11. In the molecular packing of **1**, each independent molecule self-associates into a dimeric aggregate via hydroxy-O–H···N(imine) hydrogen bonds as shown in Fig. 5(a) and Fig. SI 8(a) for the first and second independent molecules, respectively. The supramolecular dimers are assembled into a layer in the ab-plane via furanyl- and imine-C–H···O(oxido) interactions occurring between Mo1- and Mo2-containing molecules, Fig. SI 8(b). The layers inter-digitate along the c-axis with the closest atom-to-atom contact being a weak methyl-C–H···O(oxido) contact, Fig. SI 8(c).

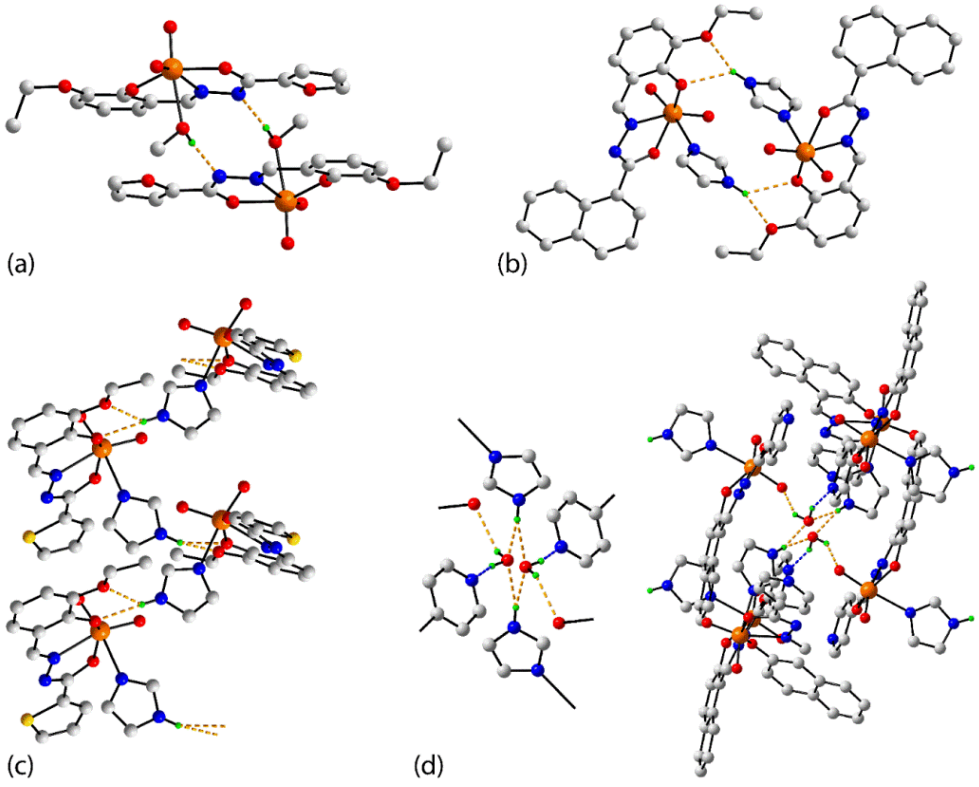

Fig. 5. Supramolecular aggregates in the crystals of **1**-**4** sustained by hydrogen bonding (shown as orange dashed lines): (a) dimer in **1** stabilised by hydroxy-O–H···N(imine) hydrogen bonds [O6–H6o···N2^{i}: H6o···N2^{i} = 1.907(19) Å, O6···N2^{i} = 2.732(2) Å with angle at H6o = 168(2)° for

symmetry operation (i) 2-x, 2-y, 1-z], (b) dimer in **2** mediated by imidazole-N–H···O(phenoxide, ethoxy) hydrogen bonds [N4–H4n···O1^{ii}: H4n···O1^{ii} = 2.28(3) Å, N4···O1^{ii} = 2.953(4) Å with angle at H4n = 133(4)°; N4–H4n···O5^{ii}: H4n···O5^{ii} = 2.26(3) Å, N4···O5^{ii} = 2.983(4) Å with angle at H4n = 139(4)° for (ii) 1-x, 1-y, 1-z], (c) helical chain in **3** sustained by imidazole-N–H···O(phenoxide, ethoxy) hydrogen bonds [N4–H4n···O1^{iii}: H4n···O1^{iii} = 2.19(3) Å, N4···O1^{iii} = 2.947(3) Å with angle at H4n = 144(3)°; N4–H4n···O5^{iii}: H4n···O5^{iii} = 2.23(3) Å, N4···O5^{iii} = 2.927(3) Å with angle at H4n = 136(3)° for (iii) -½+x, ½-y, 1-z] and (d) detailed view and seven-molecule aggregate in **4** sustained by imidazole-N–H···O(water), water-O–H···O(oxido) and water-O–H···N(pyridyl) hydrogen bonds [O1w–H1w···O3^{iv}: H1w···O3^{iv} = 2.30 Å, O1w···O3^{iv} = 3.028(5) Å with angle at H1w =145°;O1w–H2w···N5^{v}: H2w···N5^{v} = 1.91 Å, O1w···N5^{v} = 2.708(5) Å with angle at H2w =158°; N4–H4n···O1w: H4n···O1w = 1.93(2) Å, N4···O1w = 2.795(7) Å with angle at H2w = 170(4)°; N4–H4n···O1w^{vi}: H4n···O1w^{vi} = 2.16(3) Å, N4···O1w^{vi} = 3.016(7) Å with angle at H4n = 166(5)° for (iv) ½-x, -½+y, ½-z, (v) ½+x, ½-y, -½+z and (vi) -x, -y, -z]; the latter are shown as blue dashed lines. For reasons of clarity, non-participating hydrogen atoms are removed. {full page image}

Centrosymmetric supramolecular dimers are also found in the crystal of **2**. Here, the imidazole-N–H atom is bifurcated forming hydrogen bonds with the phenoxide-O1 and ethoxy-O5 atoms to form a five-membered {···H···OC$_2$O} synthon, Fig. 5(b). Each component of the dimer is connected into a layer in the ab-plane by naphthyl- and imidazole-C–H···O(oxido) and methylene-C–H···O(amide) interactions resulting in a double-layer, Fig. SI 9(a). Alternatively, the packing can be described as comprising supramolecular layers sustained by the aforementioned C–H···O interactions, see Fig. SI 9(b), which are clipped into a double-layer by the N–H···O hydrogen bonds. The double-layers stack along the c-axis direction without directional interactions between them.

In the molecular packing of **3**, analogous imidazole-N–H···O(phenoxide, ethoxy) hydrogen bonding and five-membered {···H···OC$_2$O} synthons are formed as seen for **2** but, in this case, these extend to form a one-dimensional supramolecular chain as shown in Fig. 5(c). The chain is orientated along the a-axis and has a helical topology, being propagated by screw (2_1) symmetry; additional stability to the chain is provided by imidazole-C–H···O(oxido)

interactions. Chains are connected laterally to form a supramolecular layer in the ab-plane via phenyl-C–H···O(oxido) contacts, see Fig. SI 10(a). The most prominent points of contact between layers along the c-axis direction are S···O secondary bonding interactions ($S1\cdots O2^{i}$ = 3.068(2) Å for (i): 1-x, ½+y, ½-z). Such interactions are well-known but, are gaining increasing recognition for their importance in stabilising molecular packing [91-93]; a view of the unit cell contents is shown in Fig. SI 10(b).

The inclusion of a water molecule, albeit statistically disordered about a centre of inversion, provides the cohesion to the molecular packing in the crystal of **4**. The imidazole-N–H forms hydrogen bonds to each of the disordered water-O atoms, with the water-O–H donor atoms forming hydrogen bonds to oxido-O and pyridyl-N atoms. In this way, six molecules of **4** are assembled about the water molecule. As there are peripheral oxido, imidazole and pyridyl residues in the seven-molecule aggregate, a three-dimensional architecture is generated as illustrated in Fig. SI 11.

DNA Binding Studies

Absorption spectroscopic studies

Applying spectral techniques, the DNA binding affinity of the complexes **1–4** to CT-DNA was studied and the equilibrium binding constant (K_b) of the complexes to CT-DNA was established (Table 4 and Fig. 6). Complexes **1–4** exhibit absorption bands in the regions 450–400, 340–300 that are attributed to L–Mo(dπ) and LMCT transitions while bands at 260–290 nm are due to intraligand transitions [76]. On adding CT-DNA, complex **1** showed a hyperchromic shift in the L–Mo(dπ) LMCT region whereas hypochromic shifts were observed in both the 340–300 and 260–290 nm ranges; Fig. SI 12(a). For **2**–**4**, hypochromic shifts were found in all three ranges; Fig. 6 and Figs SI 12(b)–(c). Both the hyperchromic and hypochromic shifts indicate the interaction of the CT-DNA with the dioxidomolybdenum complexes. The hyper chromic shift observed may be either due to electrostatic binding of the complexes to the DNA i.e. the external contact or to the major and minor grooves of DNA [94,95]. The observed hypochromic shifts may be due to the interaction between the electronic states of ligand chromophores and the DNA bases [96-98]. The hypochromism or hyperchromism observed in these cases were used to estimate the binding strength of the complexes to the CT-DNA. For all complexes, the 260–290 nm range showed a significant hypochromism which may be due to the higher binding affinity towards CT-DNA in the lower wavelength region. The equilibrium binding constant (K_b) between CT-DNA and each of the complexes **1**–**4** was calculated using Eqn 1 (given above).

The K_b values are shown in Table 4 and revealed that **4** has the highest binding affinity of 3.57×10^4 M^{-1} and **1** has the lowest binding affinity of 9.91×10^3 M^{-1}. All complexes display moderate binding affinity, and the DNA binding strength of the complexes are in the order of **4** > **3** > **2** > **1** (Table 4). There were no significant interactions observed for the ligands towards CT-DNA.

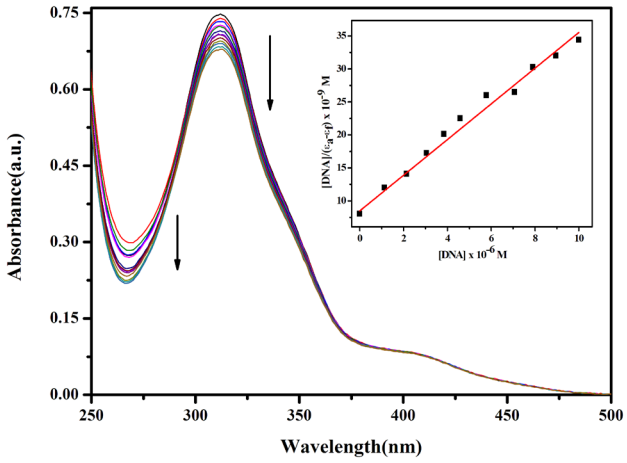

Fig. 6. Electronic absorption spectra of $[Mo^{VI}O_2L^4(Q)]_2.H_2O$ (**4**) (25 μM) upon the titration of CT-DNA (0–110 μM) in 50 mM Tris-HCl buffer (pH 8.0). The arrow indicates the changes in absorbance intensity with respect to an increase in the concentration of CT-DNA. The inset shows the linear fit of $[DNA]/(\varepsilon_a - \varepsilon_f)$ vs. [DNA].

Table 4. CT-DNA Binding parameters for complexes **1**-**4**.

Complex	Binding Constant (K_b) (M^{-1})	Bimolecular rate constant (K_q) Value($M^{-1}s^{-1}$)
1	9.91×10^3	6.25×10^{11}
2	1.49×10^4	8.16×10^{11}
3	2.61×10^4	8.58×10^{11}
4	3.57×10^4	1.27×10^{12}

Competitive Binding Studies

In an attempt to determine the exact mode of binding of the complexes to CT-DNA, competitive binding experiments were performed with three fluorescent dyes namely 4′,6-diamidino-2-phenylindole (DAPI), methyl green (MG) and ethidium bromide (EB). Among the three, EB tends to bind DNA through an intercalation mode whereas DAPI and MG bind the minor and major grooves, respectively [71]. Titration of EB with increasing concentration of complex show the quenching of emission intensity of EB bound to CT-DNA at 596 nm with a bathochromic shift. Thus, the indicated displacement of CT-DNA bound EB by **1-4** shows the binding through intercalation mode; Fig. 7 and Fig. SI 13. The bimolecular rate constant (K_q) of EB quenching was determined by following the Stern–Volmer equation and was found to be in the range 6.25 x 10^{11} − 1.27 x 10^{12} M^{-1} s^{-1} (Table 4). Further, on titration of DAPI bound CT-DNA with increasing concentration of the complexes, **1** and **3** showed the quenching of emission intensity at 451 nm with a visible hypsochromic shift, whereas **2** shows a bathochromic shift at the same range in the emission maxima (Fig. SI 14). From the data it also shows that except for **4**, **1-3** bind to CT-DNA through minor groove binding mode. All complexes exhibited the quenching of ∼53% for **1** followed by ∼56% and ∼62% for **2** and **3**, respectively at the fluorescence intensity of 451 nm. On the other hand, only for complex **4** was a proportionate binding observed on titration with MG bound CT-DNA. A bathochromic shift is observed at 663 nm, confirming the major groove binding mode of **4** to CT-DNA (Fig. SI 15). Hence, these data prove that **1**–**3** along with an intercalative mode of binding also bind to CT-DNA through minor groove binding, while **4** binds through intercalation and in the major groove binding mode.

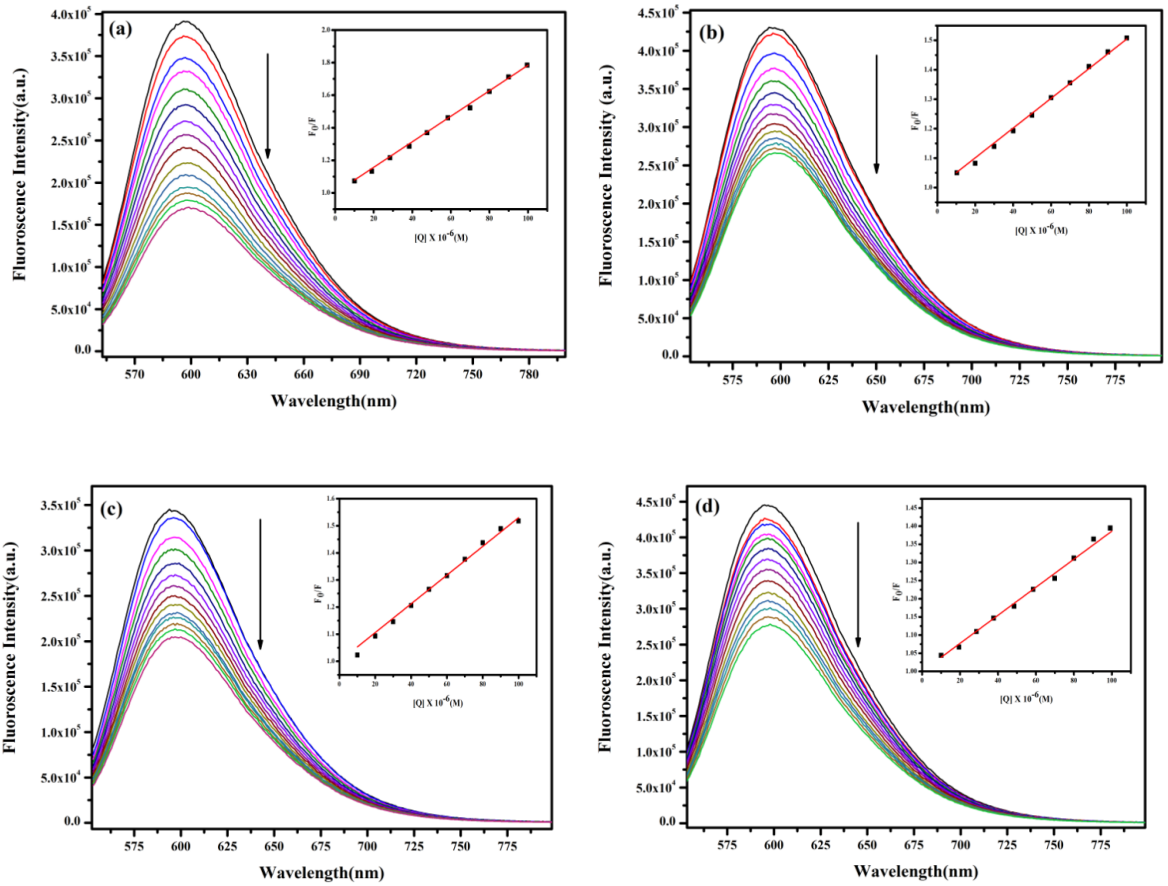

Fig. 7. Fluorescence quenching of EB (10 μM) upon the titration of complex **1** (a), **2** (b), **3** (c) and **4** (d) (0–100 μM each). The arrows indicate the decrease in fluorescence intensity with respect to an increase in the complex concentration; the inset shows the Stern-Volmer plot of the respective complexes.

In vitro cytotoxic activity

MTT assay

In order to understand the *in vitro* cytotoxic potential of the synthesized complexes, an MTT assay was performed against two cancer cell lines HT-29 and HeLa after 48 h of incubation. As the test complexes were dissolved in DMSO, DMSO was taken as a control experiment so as to identify the role of solvent in cytotoxicity of the complexes. The results obtained were analyzed through a

% cell viability profile and expressed in terms of their IC_{50} values, as depicted in Fig. 8 and Table 5. The aroylhydrazone ligands gave high IC_{50} values of > 300 μM. Among all the complexes, **4** proved to be the most active against both the cell lines. It was capable of killing almost 50% of the cell population even at a concentration of 5μg/ml. While the rest of the complexes proved to be less potent.

Lately, remarkable cytotoxic activities have been reported for molybdenum complexes against various human cancer cell lines such as A-549(lung cancer), HeLa (cervical carcinoma) and MCF-7 (breast carcinoma) [99-103]. Cytotoxicity of **4** was found to be comparable and even better than those of some clinical drugs and various previous reports of molybdenum complexes as cytotoxic agents [104-107]. After analysing both DNA binding and cytotoxicity result it was observed that among the four complexes, mixed ligand complexes **2**–**4** showed better biological activity than that of complex **1**, with a coordinated methanol moelcule. While complex **4** showed the highest cytotoxicity among the three mixed ligand complexes, probably due to the presence of heterocyclic 2-hydroxy-1-naphthyl functional group attached to the ligand backbone in comparison to **2** and **3** [32,34,108].

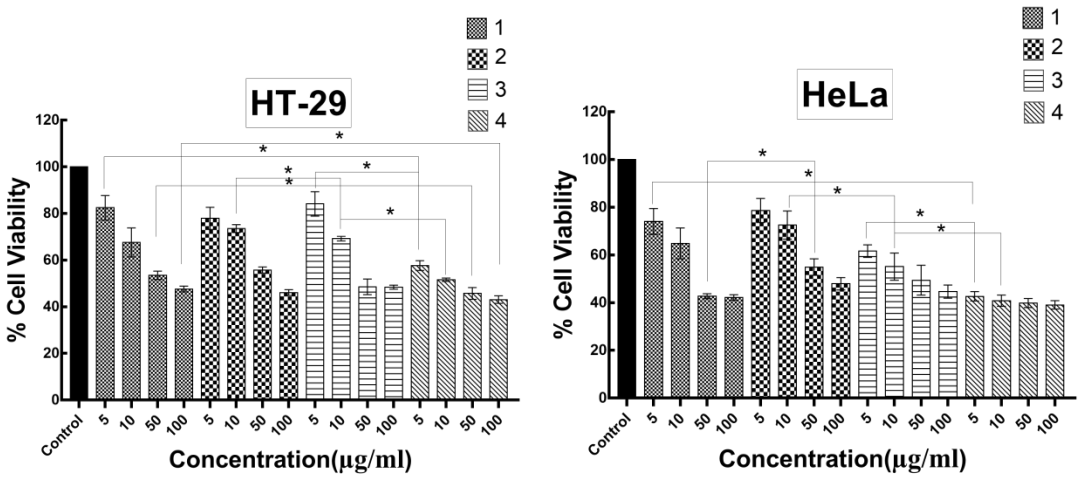

Fig. 8. Cell viability profile of 1-4 against HT-29 and HeLa after 48h of incubation. Data are reported as the mean ± SD for n = 4 and *p<0.05 statistical differences between treatment of complexes **1**–**4**.

Table 5. IC_{50} values of **1**-**4**.

Complexes	**IC_{50} (µM)**	**IC_{50} (µM)**
	HT-29	**HeLa**
1	177.92 ± 5.41	84.63 ± 3.26
2	150.89 ± 2.65	162.55 ± 1.54
3	96.26 ± 0.80	60.64 ± 3.81
4	20.63 ± 0.71	4.41 ± 0.98

DAPI Staining

As complex **4** proved to be the most potent among the series, it was logical to study its effect on the nuclear morphology of both cancer cell lines. This was studied through DAPI staining. Cells were treated at a concentration of 50 µg/ml of **4** for a period of 24 h, after which they were stained with DAPI and examined under a fluorescence microscope. From the images (Fig. 9) it could be deduced that there were condensed chromatin bodies, nuclear blebbings and shrunken morphology

in the cells treated with **4**, whereas there were hardly any condensation observed in the control image. These phenomena are indicative of apoptosis taking place as the mechanism of cell death in response to treatment with **4**.

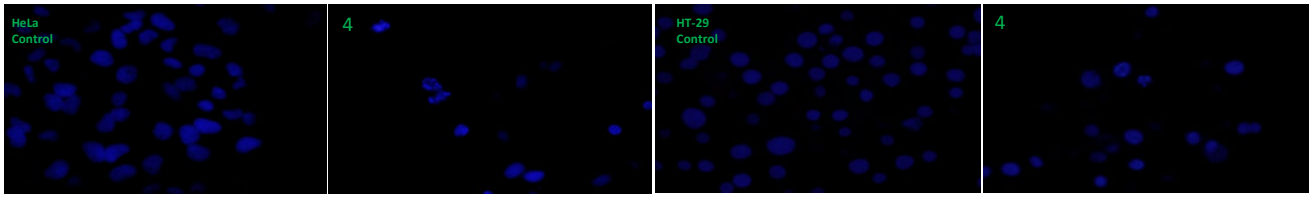

Fig. 9. Morphology of HeLa and HT-29 control and cells treated with complex **4** for 24 h. The cells were stained with DAPI and visualized under fluorescent microscope. Scale bar corresponds to 20 μm.

Conclusions

In summary, this article presents the synthesis and characterization of four new mixed ligand dioxidomolybdenum(VI) $[Mo^{VI}O_2L^{1\text{-}3}(Q)]$ **(1–3)** and $[Mo^{VI}O_2L^{4}(Q)]_2.H_2O$ **(4)** [where Q = MeOH for **1** and imidazole for **2–4**] complexes from tridentate arolyazine ligand systems ($H_2L^{1–4}$). Single crystal X-ray crystallography revealed a distorted octahedral structure in each case. Hydrogen bonding features in the molecular packing of **1–4**, lead to supramolecular dimeric aggregates in **1** and **2**, a helical chain in **3** and a three-dimensional architecture in **4**.

The present series of complexes were tested for biological properties in terms of their DNA binding ability and *in vitro* cytotoxicity. The study revealed that the complexes bind moderately with CT-DNA via intercalative, minor and major groove modes, while **4** showed the highest binding affinity compared to the other complexes. Also, the result of an antiproliferative study revealed **4** to be the most cytotoxic towards both HT-29 and HeLa cancer cell lines among the series. The presence of

imidazole as a co-ligand along with a heterocyclic 2-hydroxy-1-naphthyl moiety in the ligand backbone of **4** may be responsible for a better interaction with DNA as well as cytotoxicity in comparison to the other complexes. The outcome of the present study will definitely boost further research on the design of dioxidomolybdenum complexes as metal-based agents for anticancer studies.

Appendix A. Supplementary material

Crystallographic data for **1-4** reported in this paper have been deposited with the Cambridge Crystallographic Data Centre (CCDC) as supplementary publication nos 1920543-1920546 for **1-4**, respectively. These data can be obtained free of charge via www.ccdc.cam.ac.uk/getstructures. Geometric data characterising the chelate rings are given in Table SI 1 and crystallographic diagrams and details of the specified intermolecular interactions are given in Figs SI 7-11 whereas the spectra are given in Figs SI 1-6 and SI 12-15.

Acknowledgements

R. D thanks DBT, Govt. of India [Grant No. 6242-P112/RGCB/ PMD/DBT/RPDA/2015] and CSIR, Govt. of India [Grant No. 01(2963)/18/EMR-II] for funding this research. The authors also thank Sunway University Sdn Bhd (Grant no. STR-RCTR-RCCM-001-2019) for support of crystallographic studies.

References

1. C. Beedham, Molybdenum hydroxylases as drug-metabolizing enzymes, Drug Metab Rev 16 (1985) 119–156.
2. R.C. Bray, Quart. Rev. Biophys. 21 (1988) 299–329.
3. J.P.G. Malthouse, R.C. Bray, Biochem. J. 191 (1980) 265–267.
4. R.H. Holm, Chem. Rev. 87 (1987) 1401–1449.
5. Y.-L. Qiao, S.M. Dawsey, F. Kamangar, J.-H. Fan, C.C. Abnet, X.-D. Sun, L.L. Johnson, M.H. Gail, Z.-W. Dong, B. Yu, S.D. Mark, P.R. Taylor, J. Natl, Cancer Inst. 101 (2009) 507–518.
6. J. Honzíček, J. Vinklárek, M. Erben, Z. Padělková, L. Šebestová, M. Řezáčová, J. Organomet. Chem. 749 (2014) 387–393.
7. M.R.P. Norton de Matos, C.C. Romão, C.C.L. Pereira, S.S. Rodrigues, M. Mora, M.J.P. Silva, P.M. Alves, C.A. Reis, International Patent WO/2005/087783.
8. J. Feng, X. Lu, G. Wang, S. Du, Y. Cheng, Dalton Trans. 41 (2012) 8697–8702.
9. A.K. Sah, N. Baig, Catal. Lett. 145 (2015) 905–909.
10. Z. Hu, X. Fu, Y. Li Inorg, Chem. Commun. 14 (2011) 497–507.
11. S. N. Rao, N. Kathale, N. N. Rao, K. N. Munshi, Inorg. Chim. Acta 360 (2007) 4010–4016.
12. Y. Li, X. Fu, B. Gong, X. Zou, X. Tu, J. Chen, J. Mol. Catal. A: Chem. 322 (2010) 55–62.
13. M. Masteri-Farahani, F. Farzaneh, M. Ghandi, J. Mol. Catal. A: Chem. 248 (2006) 53–60.
14. M. Masteri-Farahani, F. Farzaneh, M. Ghandi, Catal. Commun. 8 (2007) 6–10.
15. A. Rezaeifard, I. Sheikhshoaie, N. Monadi, M. Alipour, Polyhedron 29 (2010) 2703–2709.
16. F.E. Kuhn, A.M. Santos, A.D. Lopes, I.S. Goncalves, J. E. Rodrı´guez-Borges, M. Pillinger, C.C. Roma~o, J. Organomet. Chem. 621 (2001) 207–217.

17. M. Groarke, I.S. Goncalves, W.A. Herrmann, F.E. Kuhn, J. Organomet. Chem. 649 (2002) 108–112.
18. J. Fridgen, W.A. Herrmann, G. Eickerling, A.M. Santos, F.E. Kuhn, J. Organomet. Chem. 689 (2004) 2752–2761.
19. A. Sakthivel, J. Zhao, G. Raudaschl-Sieber, M. Hanzlik, A.S.T. Chiang, F.E. Kuhn, Appl. Catal. A: Gen. 281 (2005) 267–273.
20. I.S. Goncalves, A.M. Santos, C.C. Romao, A.D. Lopes, J.E. Rodrı´guez-Borges, M. Pillinger, P. Ferreira, J. Rocha, F.E. Kuhn, J. Mol. Catal. A: Chem. 222 (2004) 265–271.
21. S. P. Dash, S. Majumder, A. Banerjee, M. F. N. N. Carvalho, P. Adão, J. Costa Pessoa, K. Brzezinski, E. Garribba, H. Reuter, R. Dinda, Inorg. Chem. 55 (2016)1165–1182.
22. S. P. Dash, S. Roy, M. Mohanty, M. F. N. N. Carvalho, M. L. Kuznetsov, J. C. Pessoa, A. Kumar, Y. P. Patil, A. Crochet, R. Dinda, Inorg. Chem. 55 (2016) 8407–8421.
23. M. Mancka, W. Plass, Inorg. Chem. Commun. 10 (2007) 677–680.
24. S. P. Dash, S. Pasayat, S. Bhakat, S. Roy, R. Dinda, E. R. T. Tiekink, S. Mukhopadhyay, S. K. Bhutia, M. R. Hardikar, B. N. Joshi, Y. P. Patil, M. Nethaji, Inorg. Chem. 52 (2013) 14096–14107.
25. S. Naskar, M. Corbella, A. J. Blake, S. K. Chattopadhyay, Dalton Trans. (2007) 1150–1159.
26. D. S. Raja, N. S. P. Bhuvanesh, K. Natarajan, J. Biol. Inorg. Chem. 17 (2012) 223–237.
27. T. B. Chaston, D. R. Richardson, J. Biol. Inorg. Chem. 8 (2003) 427–438.
28. Q. Wang, Z. Y. Yang, G. F. Qi, D. D. Qin, Biometals 22 (2009) 927–940.
29. Z. Y. Yang, B. D. Wang, Y. H. Li, J. Organomet. Chem. 691 (2006) 4159–4166.

30. B. D. Wang, Z. Y. Yang, P. Crewdson, D. Q. Wang, J. Inorg. Biochem. 101 (2007) 1492–1504.
31. T. R. Li, Z. Y. Yang, B. D. Wang, D. D. Qin, Eur. J. Med. Chem. 43 (2008) 1688–1695.
32. Q. Wang, Z. Y. Yang, G. F. Qi, D. D. Qin, Eur. J. Med. Chem. 44 (2009) 2425–2433.
33. Z. C. Liu, B. D. Wang, Z. Y. Yang, Y. Li, D. D. Qin, T. R. Li, Eur. J. Med. Chem. 44 (2009) 4477–4484.
34. Y. Li, Z. Y. Yang, M. F. Wang, Eur. J. Med. Chem. 44 (2009) 4585–4595.
35. K. Ghosh, P. Kumar, N. Tyagi, U. P. Singh, V. Aggarwal, M. C. Baratto, Eur. J. Med. Chem. 45 (2010) 3770–3779.
36. Z. C. Liu, B. D. Wang, B. Li, Q. Wang, Z. Y. Yang, T. R. Li, Y. Li, Eur. J. Med. Chem. 45 (2010) 5353–5361.
37. P. Krishnamoorthy, P. Sathyadevi, A. H. Cowley, R. R. Butorac, N. Dharmaraj, Eur. J. Med. Chem. 46 (2011) 3376–3387.
38. B. D. Wang, Z. Y. Yang, T. R. Li, Bioorg. Med. Chem. 14 (2006) 6012–6021.
39. P. Krishnamoorthy, P. Sathyadevi, R. R. Butorac, A. H. Cowley, N. S. P. Bhuvanesh, N. Dharmaraj, Dalton Trans. 41 (2012) 4423–4436.
40. M. Alagesan, N. S. P. Bhuvanesh, N. Dharmaraj, Dalton Trans. 42 (2013) 7210–7223.
41. A. C. Cunha, J. M. Figueiredo, J. L. M. Tributino, A. L. P. Miranda, H. C. Castro, R. B. Zingali, C. A. M. Fraga, M. C. B. V. Souza, V. F. Ferreira, E. Barreiro, J. Bioorg. Med. Chem. 11 (2003) 2051–2059
42. J. Easmon, G. Puerstinger, K. S. Thies, G. Heinisch, J. Hofmann, J. Med. Chem. 49 (2006) 6343–6350.

43. T. B. Chaston, R. N. Watts, J. Yuan, D. R. Richardson, Clin. Cancer Res. 10 (2004) 7365–7374.
44. V. Singh, V. K. Srivastava, G. Palit, K. Shankar, A. – Forsch, Drug. Res. 42 (1992) 993–996.
45. N. Singh, R. Ranjana, M. Kumari, B. Kumar, IJPCR 8 (2016) 162–166.
46. A. G. Tempone, R. A. Mortara, H. F. De Andrade Jr., J. Q. Reimão, Int. J. Antimicrob. Agents, 36 (2010) 159–163.
47. F. Léonard, A. Andrémont, C. Tancréde, J. Appl. Bacteriol. 58 (1985) 545–553.
48. S. Patterson, S. Wyllie, Trends Parasitol., 30 (2014) 289–298.
49. L. J. Rubin, R. H. Peter, J. Med. 302 (1980) 69–73.
50. S. Todorovic, N. Juranic, S. Macura, F. Rusnak, J. Am. Chem. Soc. 121 (1999) 10962–10966.
51. O. Pouralimardan, A. Chamayou, C. Janiak, H. Monfared, Inorg Chim Acta 360 (2007) 1599–1608.
52. C. Basu, S. Chowdhury, R. Banerjee, H. S. Evans, S. Mukherjee, Polyhedron 26 (2007) 3617–3624.
53. M. Bakir, O. Green, W. H. Mulder, J Mol Struct. 873 (2008) 17–28.
54. P. Melnyk, V. Leroux, C. Sergheraert, P. Grellier, Bioorg. Med. Chem. Lett. 16 (2006) 31–35.
55. S. G. Kucukguzel, A. Mazi, F. Sahin, S. Ozturk, J. Stables. Eur. J. Med. Chem. 38 (2003) 1005-1013.
56. D. Sriram, P. Yoggeswari, K. Madhu, Bioorg. Med. Chem. Lett. 15 (2005) 4502–4505.

57. S. G. Kucukguzel, S. Rollas, I. Kucukguzel, M. Kiraz, Eur. J. Med. Chem. 34 (1999) 1093–1100.
58. S. Gemma, G. Kukreja, C. Fattorusso, M. Persico, M. P. Romano, M. Altarelli, L. Savini, G. Campiani, E. Fattorusso, N. Basilico, D. Taramelli, V. Yardley, S. Butini. Bioorg. Med. Chem. Lett. 16 (2006) 5384–5388.
59. F. Bellina, S. Cauteruccio, R. Rossi, Tetrahedron 63(2007) 4571–4624.
60. R. Di Santo, A. Tafi, R. Costi, M. Botta, M. Artico, F. Corelli, M. Forte, F. Caporuscio, L. Angiolella, A. T. Palamara, J. Med. Chem. 48 (2005) 5140–5153.
61. S. Dutta, Acta Pharmaceutica 60 (2010) 229–235.
62. A. Banerjee, S. P. Dash, M. Mohanty, D. Sanna, G. Sciortino, V. Ugone, E. Garribba, H. Reuter, W. Kaminsky, R. Dinda, J. Inorg. Biochem. 199 (2019) 110786.
63. M. Mohanty, S. K. Maurya, A. Banerjee, S. A. Patra, M. R. Maurya, A. Crochet, K. Brzezinski, R. Dinda, New J. Chem. (2019) 10.1039/c9nj01815h
64. S. Lima, A. Banerjee, M. Mohanty, G. Sahu, C. Kausar, S. K. Patra, E. Garribba, W. Kaminsky, R. Dinda, New J. Chem. (2019) 10.1039/c9nj01910c
65. S. Majumder, S. Pasayat, S. Roy, S. P. Dash, S. Dhaka, M. R. Maurya, M. Reichelt, H. Reuter, K. Brzezinski, R. Dinda, Inorg. Chim. Acta 469 (2018) 366–378.
66. S. Majumder, S. Pasayat, A. K. Panda, S. P. Dash, S. Roy, A. Biswas, M. E. Varma, B. N. Joshi, E. Garribba, C. Kausar, S. K. Patra, W. Kaminsky, A. Crochet, R. Dinda, Inorg. Chem. 56 (2017) 11190–11210.
67. S. P. Dash, A. K. Panda, S. Dhaka, S. Pasayat, A. Biswas, M. R. Maurya, P. K. Majhi, A. Crochet, R. Dinda, Dalton Trans. 45 (2016) 18292–18307.

68. S. Pasayat, M. Böhme, S. Dhaka, S. P. Dash, S. Majumder, M. R. Maurya, W. Plass, W. Kaminsky, R. Dinda, Eur. J. Inorg. Chem. 10 (2016) 1604–1618.
69. Saswati, A. Chakraborty, S. P. Dash, A. K. Panda, R. Acharyya, A. Biswas, S. Mukhopadhyay, S. K. Bhutia, A. Crochet, Y. P. Patil, M. Nethaji, R. Dinda, Dalton Trans. 44 (2015) 6140–6157.
70. S. P. Dash, A. K. Panda, S. Pasayat, S. Majumder, A. Biswas, W. Kaminsky, S. Mukhopadhyay, S. K. Bhutia, R. Dinda, J. Inorg. Biochem. 144 (2015) 1–12.
71. S. P. Dash, A. K. Panda, S. Pasayat, R. Dinda, A. Biswas, E. R. T. Tiekink, S. Mukhopadhyay, S. K. Bhutia, W. Kaminsky, E. Sinn, RSC Adv. 5 (2015) 51852–51867.
72. S. Pasayat, S. P. Dash, S. Majumder, R. Dinda, E. Sinn, H. Stoeckli-Evans, S. Mukhopadhyay, S. K. Bhutia, P. Mitra, Polyhedron 80 (2014) 198–205.
73. S. P. Dash, A. K. Panda, S. Pasayat, R. Dinda, A. Biswas, E. R. T. Tiekink, Y. P. Patil, M. Nethaji, W. Kaminsky, S. Mukhopadhyay, S. K. Bhutia, Dalton Trans. 43 (2014) 10139–10156.
74. S. Pasayat, S. P. Dash, S. Roy, R. Dinda, S. Dhaka, M. R. Maurya, W. Kaminsky, Y. P. Patil, M. Nethaji, Polyhedron 67 (2014) 1–10.
75. R. Dinda, P. Sengupta, M. Sutradhar, T. C. W. Mak, S. Ghosh, Inorg. Chem. 47 (2008) 5634–5641.
76. R. Dinda, P. Sengupta, S. Ghosh,, W. S. Sheldrick,. Eur. J. Inorg. Chem. 2003 (2003) 363–369.
77. R. Dinda, P. Sengupta, S. Ghosh, T. C. W. Mak, Inorg. Chem. 41 (2002) 1684–1688.
78. S. Purohit, A. P. Koley, L. S. Prasad, P. T. Manoharan, S. Ghosh, Inorg. Chem. 283 (1989) 735–741.

79. G. J. -J. Chen, J. W. McDonald, W. E. Newton, Inorg. Chem. 15 (1976) 2612–2615.
80. Rigaku Oxford Diffraction, CrysAlis PRO, Yarnton, Oxfordshire, England, 2017.
81. Agilent Technologies, CrysAlis PRO, Agilent Technologies, Yarnton, Oxfordshire, England, 2010
82. G. M. Sheldrick, Acta Crystallogr. A 64 (2008) 112–122.
83. G. M. Sheldrick, Acta Crystallogr. C 71 (2015) 3–8.
84. L. J. Farrugia, J. Appl. Crystallogr. 45 (2012) 849–854.
85. DIAMOND, Visual Crystal Structure Information System, Version 3.1, CRYSTAL IMPACT, Postfach 1251, D–53002 Bonn, Germany, (2006).
86. A. L. Spek, Acta Crystallogr. Sect. D: Biol. Crystallogr. 65 (2009) 148–155.
87. N.-ul H. Khan, N. Pandya, N. C. Maity, M. Kumar, R. M. Patel, R. I. Kureshy, S. H. R. Abdi, S. Mishra, S. Das, H. C. Bajaj, Eur. J. Med. Chem. 46 (2011) 5074–5085.
88. C. Artner, H. U. Holtkamp, C. G. Hartinger, S. M. M.-Menches, J. Inorg. Biochem. 177 (2017) 322–327.
89. S. Das, G. P. Muthukumaragopal, S. N. Pal, S. Pal, New J. Chem. 27 (2003) 1102–1107.
90. R. Dinda, P. Sengupta, S. Ghosh, H. Mayer-Figge, W. S. Sheldrick J. Chem. Soc., Dalton Trans. (2002) 4434–4439
91. N.W. Alcock, Adv. Inorg. Chem. 15 (1972) 1–58.
92. E.R.T. Tiekink, Coord. Chem. Rev. 345 (2017) 209–228.
93. L. Vogel, P. Woner, S.M. Huber, Angew. Chem. Int. Ed. 58 (2019) 1880–1891.
94. M. Sakthi, A. Ramu, J. Mol. Struct. 1149 (2017) 727–735.
95. I.M. El-Deen, A.F. Shoair, M.A. El-Bindary, J. Mol. Struct. 1180 (2019) 420–437.
96. F. Arjmand, B. Mohani, S. Ahmad, Eur. J. Med. Chem. 40 (2005) 1103–1110.

97. V. Rajendiran, M. Murali, E. Suresh, S. Sinha, K. Somasundaram, M. Palaniandavar, Dalton Trans. (2008) 148–163.

98. F. Arjmand, M. Aziz, Eur. J. Med. Chem. 44 (2009) 834–844.

99. V. Vrdoljak, I. Đilović, M. Rubčić, S. K. Pavelić, M. Kralj, D. M. Čalogović, I. Piantanida, P. Novak, A. Rožman, M. Cindrić, Eur. J. Med. Chem. 45 (2010) 38−48

100. M. S. Saraiva, S. Quintal, F. C. M. Portugal, T. A. Lopes, V. Félix, J. M. F. Nogueira, M. Meireles, M. G. B. Drew, M. J. Calhorda, J. Organomet. Chem. 693 (2008) 3411−3418.

101. Y. Jin, H. Lee, M. Pyo, M. S. Lah, Dalton Trans. (2005) 797–803.

102. M. A. Hussein, T. S. Guan, R. A. Haque, M. B. K. Ahamed, A. M. S. A. Majid, Polyhedron 85 (2015) 93−103.

103. H. Thomadaki, A. Karaliota, C. Litos, A. Scorilas, J. Med. Chem. 50 (2007) 1316–1321.

104. A. Lewis, L. Forrester, J. Hayes, C. Wareing, J. Carmichael, A. Harris, M. Mooghen, C.R. Wolf, Brit. J. Cancer. 60 (1989) 327–331.

105. K. Takara, T. Sakaeda, T. Yagami, H. Kobayashi, N. Ohmoto, M. Horinouchi, K. Nishiguchi, K. Okumura, Biol. Pharm. Bull. 25 (2002) 771–778.

106. L. Reytman, O. Braitbard, E.Y. Tshuva, Dalton Trans. 41 (2012) 5241–5247.

107. A. Stockert, D. Kinder, M. Christ, K. Amend, A. Aulthouse, Austin J. Pharmacol. Ther. 2 (2014) 6.

108. D. S. Raja, N. S. P. Bhuvanesh and K. Natarajan, J. Biol. Inorg. Chem. 17 (2012) 223–237.